Decoupling the relative rate of hydrogen uptake via convection and mass transfer by a single catalytic pellet in a scaled down trickle bed reactor

Jonathan Paul White[a], Thomas William Chamberlain[b], Richard Anthony Bourne[a,b], David Taylor[c], Colin Brennan[c], Frans Muller[a,b] *

[a] School of Chemical and Process Engineering, University of Leeds, Leeds LS2 9JT, United Kingdom

[b] School of Chemistry, University of Leeds, Leeds LS2 9JT, United Kingdom

c Syngenta, Jealott's Hill International Research Centre, Berkshire RG42 6EY, United Kingdom

Abstract

Heterogenous hydrogenations of high value chemicals are a widely used class of reaction that potentially benefit from the advantages continuous processing possesses. Trickle bed reactors offer a viable alternative to batch manufacture, however further understanding of the interplay between hydrogen masstransfer and catalytic reaction is required to facilitate the uptake of such technologies.

To isolate the transport processes, the hydrogenation of styrene was conducted with a single 1% palladium on carbon pellet was immobilized within glass beads with a liquid feed either hydrogen saturated or hydrogen free and the liquid flow rate was varied. The transfer rate of hydrogen was found to be significantly affected by the hydrogen content in the feed. The observations are well described by a new model in which the pellet film is treated as a plug flow reactor, with mass transfer from the gas phase to the film modelled as diffusion through a stagnant film, and mass transfer from the film to the catalyst surface and the subsequent reaction modelled as resistances in series.

Our findings indicate that the provision of inert mass transfer area to saturate the fluid with hydrogen can significantly increase the productivity per unit mass of catalyst. In addition by

controlling the ratio of catalytic and inert surface the hydrogen concentration close to the catalyst surface can be tuned. This could be utilised to adjust both the activity and selectivity of the system and, therefore, give trickle bed reactors an advantage in chemical manufacturing processes.

Keywords

Heterogeneous hydrogenation, Mass transfer, Trickle bed reactors, Scaling down, Single pellet

Nomenclature

A_b	Surface area of a single glass bead (m^2)
A_{bs}	Total surface area of the film over the inert glass beads (m^2)
A_p	Surface area of the catalyst pellet (m^2)
A_{Pd}	Surface area of a palladium nanoparticle (m^2)
$C_{ethylbenzene}$	Concentration of ethylbenzene (mol m^{-3})
C_f	Average hydrogen concentration of the liquid film flowing over the pellet (mol m^{-3})
$\overline{C_f}$	Characteristic hydrogen concentration of the liquid film flowing over the pellet (mol m^{-3})
C_{in}	Hydrogen concentration in the liquid feed (mol m^{-3})
C_L	Hydrogen concentration in the liquid phase (mol m^{-3})
C_s	Hydrogen concentration at the surface of the catalyst (mol m^{-3})
C_0	Hydrogen concentration in the liquid at the point where the liquid reaches the pellet in the bed (mol m^{-3})
C^*	Equilibrium concentration of hydrogen in the liquid at the conditions investigated (mol m^{-3})
d_{bs}	Diameter of a single glass bead (m)
d_{Pd}	Palladium nanoparticle diameter (m)

d_{50}	The dimension that 50% of the samples dimensions are both smaller and larger than
D_{eff}	Effective diffusion rate of hydrogen in palladium on carbon catalysts ($m^2\ s^{-1}$)
$\mathbb{D}_{H_2}$	Diffusion coefficient of hydrogen in liquid ($m^2\ s^{-1}$)
g	Gravitational acceleration ($m\ s^{-2}$)
H	Henry's constant ($Pa\ m^3\ mol^{-1}$)
k_b	Liquid film mass transfer coefficient over the bead section ($m\ s^{-1}$)
$k_{b.ref}$	Mass transfer coefficient over the beads at the reference flowrate ($m\ s^{-1}$)
k''_{obs}	Observed rate constant per unit area of pellet ($m\ s^{-1}$)
k_{obs}^{Vshell}	Observed rate constant within the enriched palladium shell (s^{-1})
l_p	Catalyst pellets' length (m)
l_{unit}	Length of palladium unit cell (nm)
MTR''_{g-f}	Mass transfer flux from the gas liquid interface to the liquid film ($mol\ m^{-2}\ s^{-1}$)
MTR''_{f-s}	Mass transfer flux from the liquid film to the catalyst surface ($mol\ m^{-2}\ s^{-1}$)
MTR''_{f-R}	Mass transfer flux from the liquid film to the catalyst surface and subsequent chemical reaction ($mol\ m^{-2}\ s^{-1}$)
MTR''_{H_2}	Overall mass transfer rate of hydrogen ($mol\ m^{-2}\ s^{-1}$)
MTR''_{conv}	Convective transport of hydrogen flowing onto the pellet ($mol\ m^{-2}\ s^{-1}$)
MTR''_{radial}	Radial transport of hydrogen from the gas phase through the liquid film to the surface of the catalyst ($mol\ m^{-2}\ s^{-1}$)
N_{atoms}	Number of palladium atoms per nm^2
N_{bs}	Number of glass beads in the bed prior to the pellet
$\dot{N}_{H_2}$	Number of moles of hydrogen consumed per second at the surface of the catalyst ($mol\ s^{-1}$)
N_s	Number of palladium surface atoms per nanoparticle

P_{H_2}	Partial pressure of hydrogen (MPa)
$Pd_{\%s}$	Fraction of palladium in the enriched layer
U_{bs}	Liquid velocity over the glass beads (m s^{-1})
r_p	Radius of the catalyst pellet (m)
$R_{H_2}^{Pd}$	Rate of hydrogen consumption in terms of the catalyst weight (m^3 g^{-1} s^{-1})
S	Cross-sectional area of the reactor (m^2)
$t_{residence\ pellet}$	Residence time of the liquid over the pellet (s)
T	Temperature (K)
V_F	Volume of free space when packed (void volume)
V_R	Volume of empty reactor
V_z	Liquid velocity in the direction of gravitational force, z (m s^{-1})
W_p	Quantity of palladium in the pellet (g)
z_B	Packed bed length (m)
$\#_{Pd_{Core}}$	Number of palladium Lα counts per μm^3 in the interior of the pellet
$\#_{Pd_{Shell}}$	Number of palladium Lα counts per μm^3 in the enriched shell of the pellet

1 *Greek letters*

α	Fraction of the liquid film that forms the gas to liquid film transport resistance
β_{dyn}	Dynamic liquid holdup (m^3 liquid · m^{-3} voids)
β_{st}	Static liquid holdup (m^3 liquid · m^{-3} voids)
γ_1	Gradient of the effect of flowrate on mass transfer to beads
γ_2	Ratio of liquid film thickness over a pellet in a bed vs liquid film thickness (δ) over a pellet stack
γ_3	Liquid bypass factor
δ	Liquid film thickness
δ_b	Liquid film thickness over the glass beads (m)

δ_s	Depth of palladium enriched shell into pellets' interior (µm)
ϵ_B	Bed porosity
μ	Dynamic viscosity (kg m^{-1} s^{-1})
π	Constant; ratio of a circle's circumference to its diameter
ρ	Density of liquid (kg m^{-3})
τ	Liquid residence time in the reactor (s)
φ	Volumetric liquid flow rate (m^3 s^{-1})
φ_{ref}	Reference liquid flow condition (m^3 s^{-1})
Ω_f	Gas to liquid film transport resistance (s m^{-1})
Ω_{f-s}	Liquid Film to catalyst surface transport resistance (s m^{-1})
Ω_R	Chemical reaction resistance (s m^{-1})

Dimensionless numbers

$Re = \frac{\delta \rho V_z}{\mu}$	Reynold's number for a falling film
$Re_{bs} = \frac{\rho U_{bs} N_{bs} d_{bs}}{\mu}$	Reynold's number of the liquid over the length of the glass beads
M_T	Thiele modulus; ratio between the rate of reaction and diffusion in porous media
$Sc = \frac{\mu}{\rho \cdot \mathbb{D}_{H_2}}$	Schmidt number

1 Introduction

Heterogeneous hydrogenations are an important class of three phase catalytic reactions, used extensively within the pharmaceutical, agrichemical and other fine chemical industries. In the pharmaceutical industry alone, it has been estimated that twenty percent of all reaction steps are catalytic hydrogenations (1). Moreover, catalytic hydrogenations have been highlighted as a

potential reaction class that could significantly benefit from moving towards continuous processing to exploit the following advantages; (i) improved process safety, (ii) increased catalyst utility and (iii) finer control of hydrogen mass transfer leading to improved selectivity (2).

Trickle bed reactors represent a viable processing technology, whereby a continuous gas phase and dispersed liquid phase pass concurrently through a stationary bed of catalyst particles. The use of trickle bed reactors in the manufacture of fine chemicals offers many advantages such as liquid plug flow behaviour, reduced back mixing leading to unwanted by-products and the ability to manipulate the liquid flow rate according to heat and mass transfer resistances (3).

There exists however, a complex relationship between the hydrodynamics and kinetics that makes the physical transport and chemical processes relatively challenging to study, particularly at laboratory scale. In addition, the space and mass velocities do not scale linearly with geometry, making both scaling down and up problematic (4). Generally, two approaches to scaling down trickle bed reactors have been reported in the literature (5). The first being the design of a laboratory scale reactor that maintains hydrodynamic similarity, of which Medoras *et al*. presents an extensive review (3). The second approach is the design of a reactor for the purpose of assessment and manipulation of specific transport phenomena so as to determine the impact on the reaction. Given the nature of the work in this study, focus will be on literature in relation to the latter of the two approaches.

The second approach is illustrated by Satterfield *et al.* (6) who created a vertical 'string' of fourteen spherical catalyst pellets ($d_p = 8$ mm) to study the hydrogenation of α-methylstyrene . They compared the experimental hydrogen uptake rates to those predicted by detailed hydrodynamic models. An alternate concept is that of 'string reactors': single channels containing catalyst particles with sizes similar to the channel dimensions to create 'strings' of successive pellets. Bauer and Hasse used a string reactor ($d_p = 1.6$ mm) and compared this with a conventional trickle bed reactor using the hydrogenation of α-methylstyrene (7). The string reactor was shown to outperform

the trickle bed reactor in terms of production rate per unit mass of catalyst by a factor of up to 2 to-5. A group from Dresden has looked extensively at the mass transfer characteristics during hydrogenation of α-methylstyrene in string reactors. Using the same palladium on alumina spherical catalyst ($d_p = 0.8$ mm), different ratios of reactor to particle diameter were studied (1.25 (8), 1.76 (9) and 2.5 (10)). These studies show that mass transfer rate of hydrogen increases with superficial velocities. At high superficial velocities the mass transfer rates increase significantly with the gas volume fraction. The authors postulate that this is the result of direct transfer from the gas to the solid and demonstrates the significance of the liquid film mass transfer resistance. Kallinikos and Papayannakos employed a spiral of cylindrical extrudates rather than a vertical column for the reduction of benzene (11). They also showed the impact of the gas volume fraction, though in their case reaction limitation occurred at the higher volume fractions.

There are a relatively small number of reported instances in the literature illustrating the use of a single catalyst pellet or particle to investigate heterogeneous catalysis. With none found outlining the use of a single catalyst pellet to isolate or study the mass transport phenomena occurring in packed beds. Though described as a string pellet reactor, Hipolito *et al.* hydrogenated α-methylstryene using a single extrudate immobilised by glass beads in a horizontal pipe (12). It was identified that by varying the liquid feed rate whilst ensuring a constant liquid hourly space velocity (LHSV that the reaction was kinetically limited, as varying the feed rate had no impact on the conversion trends. Many other single pellet studies focus on the internal mass transfer resistances (pore diffusion) in what are described as diffusion reactors (13-15). All other studies have focussed on the use of single pellets to further understand heat transfer in packed bed reactors. Adaje and Sheintuch suspended a single 3.2 mm catalyst extrudate onto a thermocouple to monitor the temperature gradients and compared this to a pellet embedded in a shallow bed of inert extrudates (16). The authors speculate whether single pellet studies are suitable in determining the behaviour of an actual packed bed reactor. Watson and Harold also freely suspended a catalyst extrudate via a harness attached to a weighing balance so that the liquid holdup could be continually monitored (17). The hydrogenation of α-

methylstyrene and cyclohexane were chosen as model systems and vapourisation of the liquid phase due to the reaction was studied from the holdup data.

In this study a methodology of scaling a trickle bed reactor down to a single catalyst pellet immobilised in a vertical bed of glass beads will be presented. With the objective of investigating diffusion through the liquid film during the hydrogenation of styrene. Styrene was selected as the model system as the intrinsic chemical reaction is kinetically fast so that the external mass transfer processes can be studied (12). The aim of the work is to ascertain the limiting mechanism occurring during hydrogenations in trickle bed reactors by altering the liquid flow rate and liquid feed conditions. Gas velocity and its effect on the mass transfer of hydrogen will not be considered here. It is the final intention to develop a model that can describe the convective and radial transport of hydrogen onto the pellet, and how it affects the concentration in the liquid film close to the catalyst surface. Knowledge of such transfer mechanisms is essential in controlling the rate of supply of hydrogen to the catalyst surface, and potentially the selectivity of a reaction independent of scale.

2 Materials and Methods

2.1 Materials and Methods

Styrene 99%, methanol 99.9% and n-decane 99% were purchased from Sigma-Aldrich and used as the substrate, solvent and internal standard for subsequent gas chromatography (FID) analysis of the collected samples. 1% palladium on activated carbon extrudates Type 783 (length $d_{50} = 3.07 \pm 0.86$ mm, diameter $d_{50} = 1.65 \pm 0.16$ mm) were purchased from Johnson Matthey and the equivalent non-active carbon support (length $d_{50} = 3.66 \pm 0.86$ mm, diameter $d_{50} = 1.97 \pm 0.21$ mm) was additionally obtained for the liquid thickness experiments. A 5% palladium on activated carbon paste (Type 87L) was purchased from Johnson Matthey. To create the bed which the immobilised pellet would be placed, Ballotini solid soda glass beads (diameter 2.85–3.3 mm) were purchased from Sigmund Lindner GMBH. The aqua regia used in the inductively coupled plasma mass spectroscopy (ICP-MS) sample preparation was prepared by mixing nitric acid (68 wt %)

and hydrochloric acid (20 wt %), purchased from Fisher Chemical. All reagents and catalysts were used as received without further purification.

2.2 Palladium percentage loading of catalysts

ICP-MS as used to determine the Pd content of all catalyst materials. To circumvent issues with digestion of the carbon, the support was first crushed into a fine powder and fully oxidised by thermal degradation (18). The remaining residual powder was digested in aqua regia overnight under normal temperature and pressure conditions (21 °C and 1 bara). Ultrapure water (18 mΩ) was added to make up a diluted aqua regia solution (2.5 % v/v) which was subsequently run on a Perkin Elmer SCIEX - ELAN DRC-e, Axial Field Technology ICP-MS. A series of palladium calibration solutions were made (between 0.1 – 10 mg L^{-1}) with aqua regia in water (2.5 % v/v), yielding a linear plot with an R^2 coefficient of 0.9999.

2.3 Palladium nanoparticle size distribution

Transmission electron microscopy (TEM) was used to determine the size of the Pd nanoparticles in the catalyst. The outer layer of the 1% Pd/C pellets were removed using a scalpel and dispersed in isopropanol ($\sim$10 mL) using an ultrasonic bath. After 10 minutes, approximately 1 mL of the dispersed carbon solution was diluted again in isopropanol ($\sim$10 mL) and placed in the ultrasonic bath for 10 minutes. This solution was spotted onto a lacey carbon coated copper TEM grid mounted on filter paper until the paper became discoloured and was then left to dry. The 5% Pd/C powder was prepared is a similar manner except, rather than using a scalpel, 1 mg of the powder was dispersed in isopropanol before spotting. A 200 kV FEI Tecnai F20 FEGTEM was used to analyse the nanoparticle distribution of each sample.

2.4 Palladium location on the support

Scanning electron microscopy (SEM), coupled with energy dispersive X-ray analysis (EDX) was utilised to determine the location of the palladium within the catalyst pellets. A small sample of both the 1% Pd/C and carbon pellets were collected and each mechanically broken roughly in half

creating two separate stubs to reveal a cross section for analysis. The broken stubs were glued onto a SEM grid and analysed using a Hitachi SU8230 Scanning electron microscope 15.0 kV beam to locate the palladium. A series of 1D linescan measurements were made to obtain palladium distribution as a function of beam displacement into the pellet from the surface.

2.5 Liquid film thickness

The non-active carbon extrudates were used to mimic the 1% Pd/C in the film thickness experiments due to their pyrophoric nature and therefore, the two materials physical properties were compared before use. A complete comparison of the pellet size distributions, surface area and pore size distributions can be found in the supplementary information.

To measure the film thickness during flow, a continued surface of material for the liquid to flow down was created by forming a vertical stack of carbon pellets (height 425 mm and diameter 1.49 mm) using Araldite Standard 2-part epoxy adhesive to bind the pellets together. Under normal temperature and pressure conditions (21 ^{o}C and 1 bara), a HPLC pump (Knauer 100Smartline) was used to distribute methanol from a needle tip over the stack. A Veho VMS-004 Discovery Deluxe USB Microscope filmed the liquid flow over the pellets at the bottom of the stack; this was used as the measurement area throughout the experiment. Liquid flow rates of 0.2 – 10 mL / min were chosen, which were identified to be within the laminar flow regime using their respective Reynolds numbers ($0 < Re < 60$), no pronounced rippling was visually observed. The methanol continually flowed over the stack for 5-10 mins before recording began to ensure a constant flow regime had been established. The liquid film thickness over the pellets was determined by post-processing the recorded images via the image analysis software ImageJ. A schematic of the experimental set-up and the glued pellet stack is shown in Figure 1.

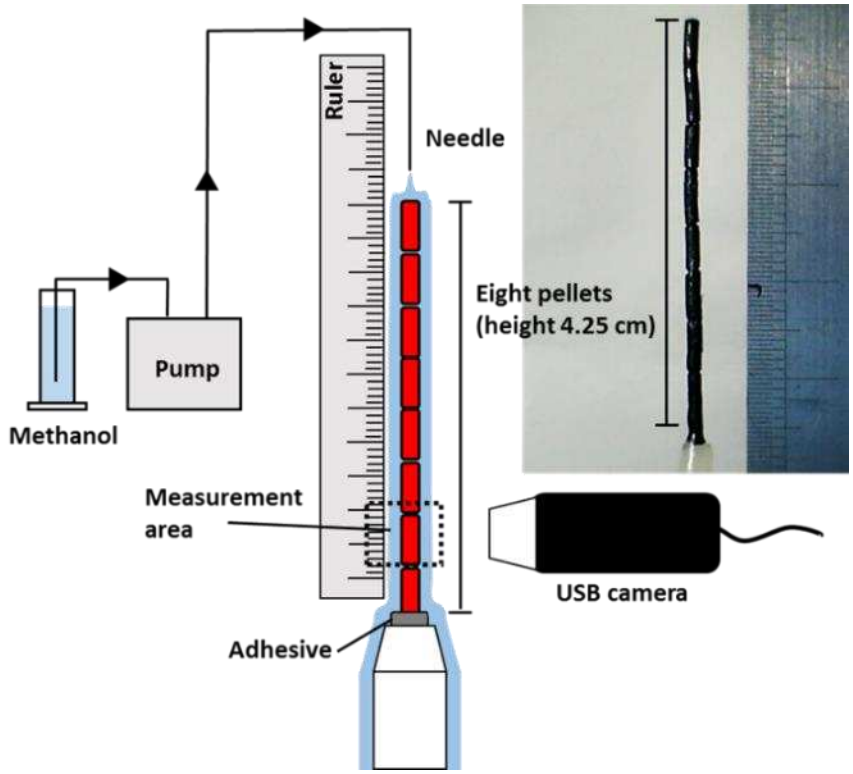

Figure 1: Schematic of the liquid film experimental setup and a picture of the glued pellets forming the stack before methanol flowed over.

The film thickness was modelled via a momentum balance of a film of uniform thickness δ flowing down over an ideal vertical cylinder (the pellet) of radius r_p. The fluid, is an incompressible fluid with constant density and viscosity. For fully developed laminar flow profile of thin films where $\delta \ll r_p$;

$$\mu \frac{\partial V_z}{\partial x} = (\delta - x)\rho g \qquad (1)$$

Where μ is the dynamic viscosity of methanol ($5.79\ x10^{-4}$ kg m^{-1} s^{-1}), ρ the density of methanol (792 kg m^{-3}), g the gravitational acceleration. Integration of Eq. (1) assuming 'no slip' at both the solid-liquid interface ($x = 0$) and the air fluid interface $x = \delta$ gives the velocity profile V_z(x). The volumetric flowrate is calculated by integration of the velocity profile with x, and for a given film thickness this can be rearranged to give Eq. **Error! Reference source not found.**, the liquid film thickness δ as function of the volumetric flow rate φ:

$$\delta = \sqrt[3]{\frac{3\varphi\mu}{2\rho g\pi r_p}} \qquad (2)$$

Lin and Liu (19) derived general laminar velocity profile for any value of δ and r_p;

$$V_z = \frac{\rho g}{4\mu}\left(\left(r_p^2 - (r_p + x)^2\right) + 2\left(r_p + \delta\right)^2 \ln\left(\frac{r_p + x}{r_p}\right)\right) \qquad (3)$$

Integration of Eq. 3 gives the volumetric flow rate;

$$\varphi = \frac{\pi\rho g\left(r_p + \delta\right)^4}{\mu}\left(\frac{1}{2}\ln\left(\frac{r_p + \delta}{r_p}\right) - \frac{1}{8}\frac{r_p^4}{\left(r_p + \delta\right)^4} + \frac{1}{2}\frac{r_p^2}{\left(r_p + \delta\right)^2} - \frac{3}{8}\right) \qquad (4)$$

The film thickness δ in Eq. 4 was determined for a given flowrate and pellet diameter using the Solver functionality in Microsoft Excel.

2.6 Single pellet reactor

Figure 2 illustrates the reactor setup for the single pellet reactor used throughout this work. The reactor itself was constructed from a glass Pasteur pipette (6.5 mm internal diameter and 104 mm length) which contained a single 1% Pd/C pellet (1.49 mm diameter, 5 mm length, 0.008 g) immobilised in a bed of glass beads (2.301 g, 80 mm bed height). The single pellet was situated 30 mm from the bottom of bed. The tip of the pipette was carefully removed to prevent liquid holdup and subsequent flooding of the bed. Carbon extrudates (0.126 g) were placed on top of the glass beads to reduce liquid mal-distribution. Cotton wool was used as a frit plate to support the bed in the pipette. The lower section of the glass pipette was bound in PFTE gas tape and placed inside a gas condenser to form a seal that forced gas flow through the bed. A needle centred directly above the bed was used as a liquid distributor and methanol was pumped into the bed with a HPLC pump (Knauer 100Smartline). Due to the low liquid flow rates required, the feed was pressurised and a 17.2 barg fixed backpressure valve was added. This greatly improved the accuracy of the flow rates without detrimentally effecting the liquid distribution from the needle tip. The hydrogen gas flow rate was regulated using a Bronkhorst mass flow meter and kept constant at 300 mL/min (superficial

gas flow rate through the bed 0.15 m/s, 0.012g m^{-2} s^{-1}) throughout all experiments. A detachable pipe, connecting the bottom of the gas condenser to a product collection vessel was used to sample during operation.

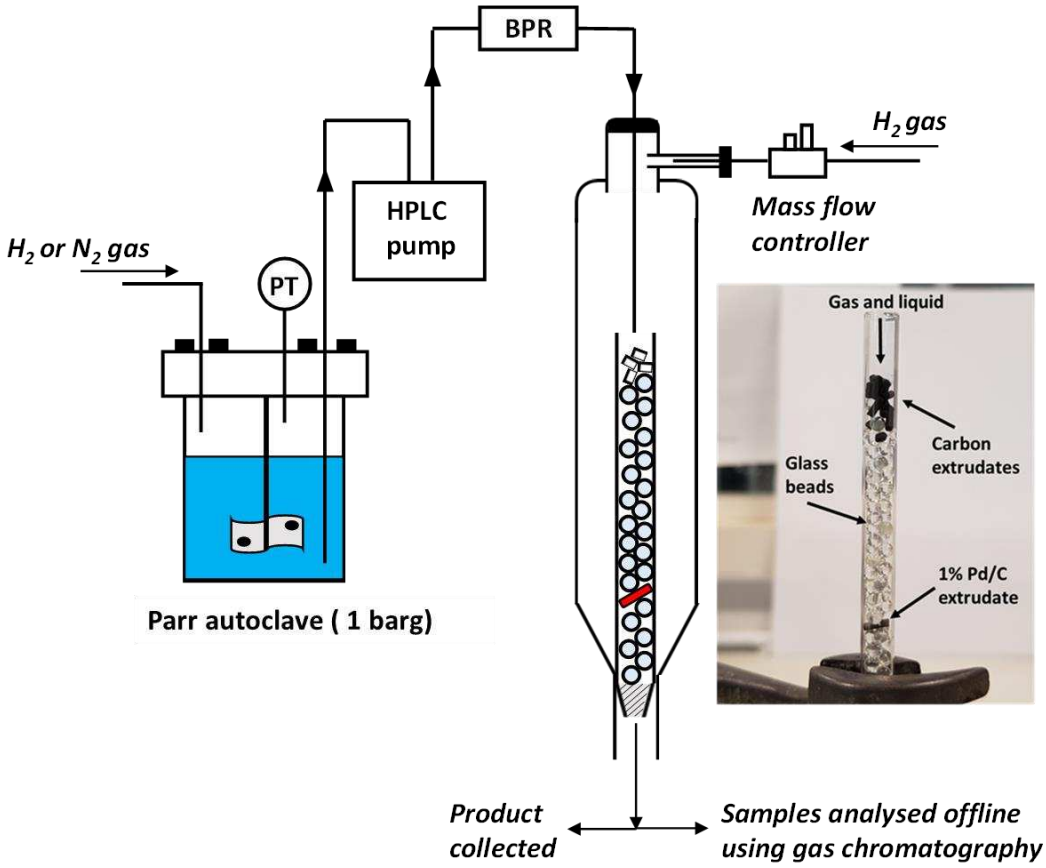

Figure 2: A schematic of the single pellet reactor experimental set-up and picture of the 1% Pd/C pellet immobilized in the bed of glass beads.

2.7 Bed porosity, liquid holdup and residence

The volume draining method (20) was used to determine the total liquid holdup in the reactor during operation. The total liquid holdup is the ratio of the volume of liquid to the total bed volume, made up of a dynamic portion of liquid, β_{dyn}, moving through the bed and a static portion of liquid retained by the bed, β_{st}. To obtain the dynamic and static liquid holdup portions, the packed glass pipette was first weighed before hydrogen gas and methanol were passed through the column concurrently for 20 minutes to reach steady-state. The flow of gas and liquid was then abruptly shut off and the liquid that freely drained from the reactor was measured and taken as the dynamic

portion. To calculate the static liquid holdup the reactor was then re-weighed and the increase in mass was attributed to the portion of liquid remaining within. Bed porosity, ϵ_B was determined by charging the reactor with methanol to calculate the volume of the empty reactor, V_R, and the volume of the free space when the reactor is fully packed, V_F;

$$\varepsilon_B = \frac{V_F}{V_R} \quad (5)$$

2.8 Hydrogenation of styrene

Assembling the reactor as described in Figure 2, exactly one 1% Pd/C pellet (0.008 mg, d_p = 1.49 mm, $l_p = 5\ mm$) was placed within the bed of glass beads. The hydrogenation of styrene was conducted as follows;

Catalyst activation: Methanol was passed through the bed and allowed to flood the bed to above the pellet to ensure complete wetting; this was repeated three times. After draining, methanol (5 mL/min) and nitrogen were passed through the reactor for fifteen minutes to purge oxygen. The gas flow was then switched to hydrogen (300 mL min^{-1}) at 21°C for a further 20 mins to activate the catalyst.

Hydrogen free feed: A styrene solution (0.18 M, 55 mmols in 0.3 L methanol with n-decane (0.025 M, 7.4 mmols) as internal standard) was fed at 1 mL / min for 10 minutes before being changed to the desired flow rate. The product stream was then sampled at 5 minute intervals over a 35 minute period. The liquid flow rate through the reactor was manually measured every 10 minutes and an average taken.

Hydrogen saturated feed: Methanol (0.3 L) and n-decane (0.025 M, 7.4 mmols) were charged into a 0.6 L batch stirred autoclave reactor (Parr Instrument Company, USA), and stirred under hydrogen with a gas entrainment impeller at 1000 rpm to fully saturate with hydrogen (2 bara for 30 minutes). Once fully saturated, the agitation was switched to 200 rpm and styrene was added to the autoclave to obtain a styrene solution in methanol (0.18 M, 55 mmols). The saturated solution was then used in the same manner as the hydrogen free styrene solution.

Analysis: Samples from both experiments were collected and analysed offline via gas chromatography on an Agilent HP-5 achiral column using n-decane as an internal standard (chosen as it was experimentally verified not to adsorb onto the catalyst itself).

3 Two stage mass transfer model

The feed initially flows over a nonreactive portion of the bed, resulting in hydrogen mass transfer into the liquid over the surface of the non-active beads. The hydrogen concentration in the liquid will either increase or decrease towards equilibrium (1 bara hydrogen gas pressure) depending on the initial feed conditions. Once the liquid feed reaches the pellet, reaction will occur at the surface of the pellet, resulting in depletion of the hydrogen flowing in to the pellet's film from the bead section. Additional hydrogen is simultaneously transferred into the film at the gas liquid interface over the pellets' surface.

Thus, the system treated as two successive mass transfer sections: (i) a bed consisting of 48 glass beads in which the hydrogen concentration moves from the inlet concentration C_{in} to the liquid concentration at the point where reaches it the pellet C_o. Followed by (ii) the cylindrical pellet which we assume is fully wetted with an averaged film thickness along its length.

(i) Liquid saturation with hydrogen and subsequent uptake

In the section of the bed above the pellet, liquid is held in place between the beads by capillary forces acting near the bead contact points. This portion of the liquid is referred to as the static holdup and is treated as a liquid reservoir (where $V_{film} < V_{reservior}$) that the hydrogen diffuses to via a liquid film (of thickness δ) flowing over the beads. Here we assume that the film flowing over a bead can be treated as if it's flowing over a cylinder with the same diameter as the bead and enough mixing occurs around the contact points (illustrated in Figure 3). Therefore, the total area of the film on the beads, A_{bs}, is;

$$A_{bs} = N_{bs}\, A_b \qquad (6)$$

Here A_b is the surface area of a single glass bead and N_{bs} the total number of beads in the reactor prior to the pellet. If the mass transfer coefficient changes slightly with liquid flow rate, the film mass transfer coefficient k_b can be linearised around a reference point:

$$k_b \approx k_{b.ref} \times \left[1 + \gamma_1 \frac{(\varphi - \varphi_{ref})}{\varphi_{ref}}\right] \quad (7)$$

where γ_1 and $k_{b.ref}$ are fitted parameters. The lowest flow rate was arbitrarily chosen as the reference condition $\varphi_{ref} = 0.2$ mL min^{-1}.

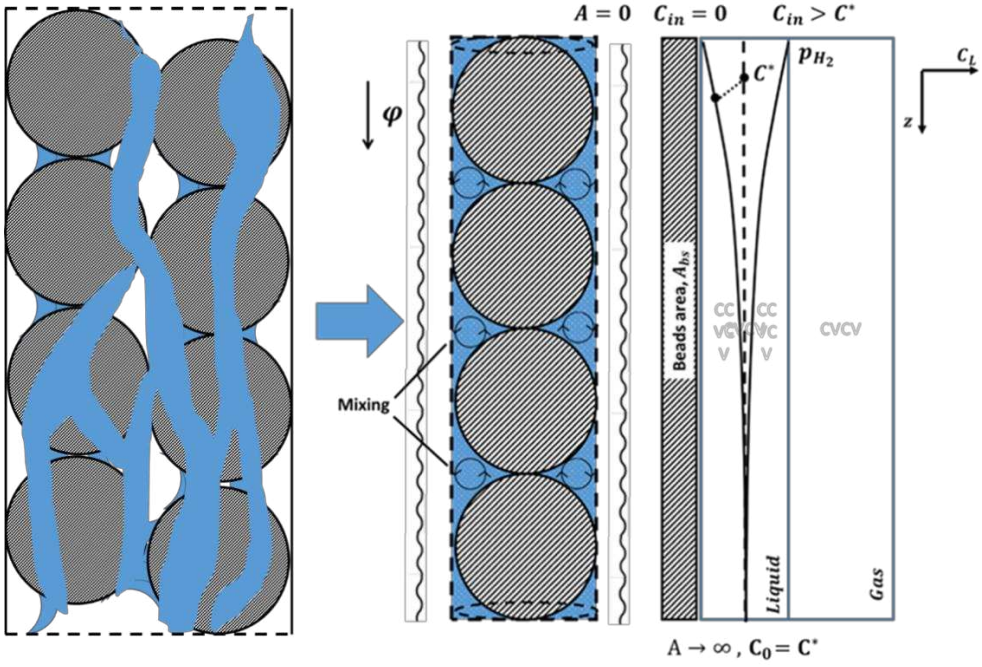

Figure 3: Schematic showing the method of modelling mass transfer of hydrogen into the liquid film on the glass beads prior to the catalyst pellet and the concentration profile in the static liquid referred to as the reservoir.

An expression of the concentration of hydrogen in the liquid, C_L is obtained following a one-dimensional steady state mass balance over section the surface area in glass beads section:

$$\varphi \, dC_L = k_b \, (C^* - C_L) \, dA \quad (8)$$

Here C^* is the equilibrium concentration of hydrogen in methanol obtained using the Henry's constant, H for hydrogen in methanol (21):

$$P_{H_2}(MPa) = H\ C^*\ with\ \ln(H) = 122.3 - 4815.6\frac{1}{T(K)} - 17.5\ln(T) + 1.4x10^{-7}P_{H2} \qquad (9)$$

Subject to the boundary condition that at $A = 0$, $C_L = C_{in}$ and $A = A_{bs}, C_L = C_0$ integrating over the full area of the glass beads gives the hydrogen concentration at the point where the liquid reaches the pellet C_o, where C_{in} is the concentration of hydrogen in the liquid feed and

$$C_0 = C^* - (C^* - C_{in})\left(e^{-\frac{k_b A_{bs}}{\varphi}}\right) \qquad (10)$$

(ii) Pellet section: Axial hydrogen concentration profile

The pellet section of the bed was modelled as a plug flow reactor, with mass transfer from the gas phase to the film modelled as diffusion through a stagnant film, and mass transfer from the film to the catalyst surface and the subsequent reaction modelled by a resistance in series model (22). This assumes the concentrations at the gas liquid interface to be in equilibrium, and that the flux of hydrogen from the gas liquid interface to the site of reaction reaches steady state instantaneously. A schematic of the pellet, the modelling methodology and the hydrogen concentration profiles in the liquid can be seen in Figure 4.

Having passed over the glass beads above, the liquid encounters the pellet with a characteristic hydrogen concentration, C_0, depending on the rate at which the liquid flows through the bed. A fraction, γ_3, of the liquid passes over the pellet, and is assumed to completely cover its surface. The remainder flows over the glass beads and the walls adjacent to the pellet. The liquid flow results in an averaged film thickness, $\gamma_2\delta$, across the length of the pellet. The parameter, γ_2, allows for an average pellet film thickness that is different, but proportional to the observed thickness as described by Eq. (2). It is assumed that within the film there is an average film concentration, C_f, that is achieved some distance, $\alpha\ \gamma_2\delta$, from the gas liquid interface. Thus, α, represents the fraction

of the liquid film that forms the gas to liquid film transport resistance, where $\alpha \leq 1$. Therefore, diffusion from the gas liquid interface to the film is then:

$$MTR''_{g-f} = \frac{1}{\alpha\Omega_f}(C^* - C_f) \quad (11)$$

Where Ω_f is the gas to liquid film transport resistance; $\Omega_f = \delta\gamma_2/\mathbb{D}_{H_2}$. Transport from the film to the catalyst surface and subsequent reaction may be described by a mass transfer in series model with two resistances: (i) diffusion from the film to the surface, Ω_{f-s} , and (ii) chemical reaction, Ω_R (where $\Omega_R = 1 \,/\, k''_{obs}$):

$$MTR''_{f-R} = \frac{1}{\Omega_{f-s}}\, C_f \;\text{ with }\; \Omega_{f-s} = (1-\alpha)\,\Omega_f + \Omega_R \quad (12)$$

Here the resistance $(1-\alpha)\,\Omega_f$ describes the flux to the catalyst surface at concentration C_S, as diffusional transport through a liquid film with thickness $(1-\alpha)\,\delta\gamma_2$:

$$MTR''_{f-s} = \frac{1}{(1-\alpha)\Omega_f}\,(C_f - C_s) \quad (13)$$

The hydrogenation of styrene may be described as proceeding via Langmuir adoption of styrene followed by subsequent hydrogenation on the surface of the palladium (23). As the styrene conversion is small (~2%) and the process is operated continuously, the reaction rate per unit pellet area is linearised with respect to the hydrogen concentration so $(-R''_S) = \left(-R''_{H_2}\right) = k''_{obs}\, C_s$ $\left(\, mol \,/\, m^2_{pellet}\; s\right)$. The mass transfer in series model assumes the rate of change of the concentration C_s is small compared to the hydrogen flux so that MTR''_{f-s}=$(-R''_s)$ and therefore Eq. 13 then follows by elimination of C_s. Finally, the film concentration C_f can be modelled by a differential molar balance over the pellet surface, da_p, yielding:

$$\gamma_3\varphi\; dC_f = \left[\frac{1}{\alpha\Omega_f}\left(C^* - C_f\right) \;-\frac{1}{\Omega_{f-s}}\, C_f\right] da_p \quad (14)$$

Integrating Eq. 14 over the area of the pellet where $C_f = C_o$ at $a_p = 0$, gives the fluid concentration of hydrogen as a function of the pellet area passed by the fluid:

$$C_f = C_\infty - (C_\infty - C_o)e^{-\frac{a_p}{A_o}} \quad with \quad C_\infty = \frac{C^*}{1 + \alpha\Omega_f/\Omega_R} \; and \; A_o = \frac{\frac{1}{\alpha\Omega_f} + \frac{1}{\Omega_R}}{\gamma_3\varphi} \qquad (15)$$

(iii) Hydrogen uptake rate on the surface of the pellet

The total rate at which hydrogen is consumed by the pellet, $\dot{N}_{H2}$, per unit time (mol/s) is given by integrating the mass transfer to the surface across the whole pellet area, A_p:

$$d\dot{N}_{H2} = \frac{1}{\Omega_{f-s}} C_f \, da_p \qquad (16)$$

Substituting Eq. 15 into Eq. 16 and integrating from $C_f = C_o$ at $a_p = 0$ gives;

$$\dot{N}_{H2} = \frac{A_p}{\Omega_{f-s}} \left[C_\infty - [\, C_\infty - \; C_0] \; \frac{A_o}{A_p} \left(1 - e^{-\frac{A_p}{A_o}} \right) \right] \qquad (17)$$

In Eq. 17, the term in the square brackets represents the characteristic hydrogen concentration in the liquid film:

$$MTR''_{H_2} = \frac{\dot{N}_{H2}}{A_P} = \frac{1}{\Omega_{f-s}} \overline{C_f} \;\; with \; \overline{C_f} = \left[1 - \left[1 - \frac{C_0}{C_\infty} \right] \frac{A_o}{A_p} \left(1 - e^{-\frac{A_p}{A_o}} \right) \right] \times C_\infty \qquad (18)$$

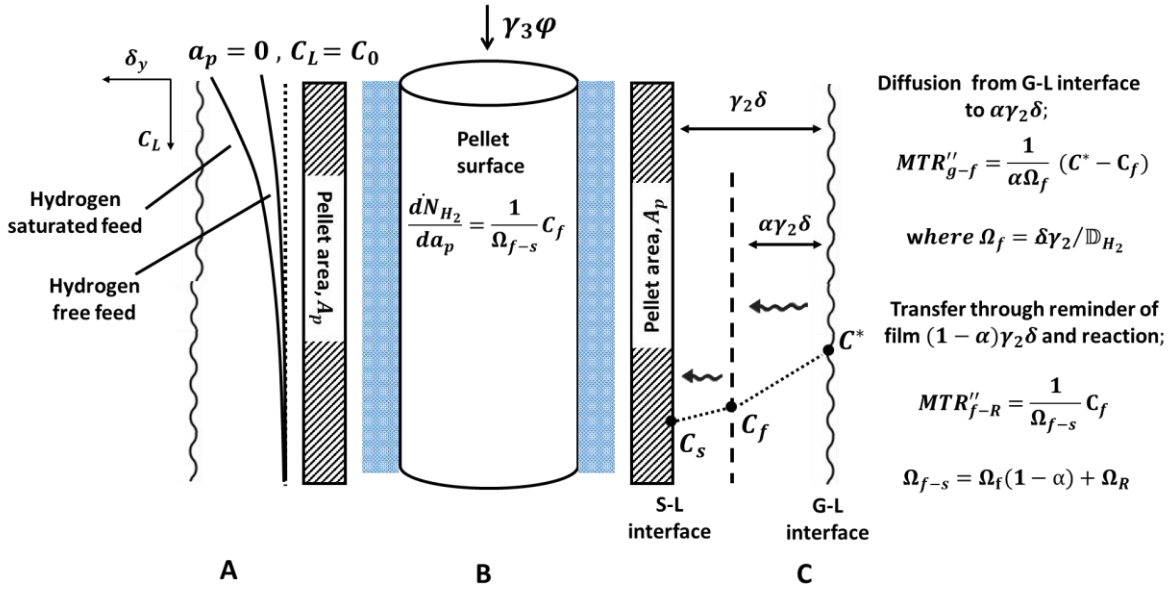

Figure 4: Diagram illustrating (A) the hydrogen concentration profile in the liquid film over the pellet, (B) a schematic of the pellet and (C) the method in which the hydrogen concentration in the film close to the surface of the pellet was modelled.

4 Results and discussions

4.1 Palladium loading, nanoparticle size distribution and location

To accurately compare the rate of reaction from pellet to pellet, the exact percentage loading must be known. The palladium loading, as measured by ICP-MS, varies from pellet to pellet, with an average loading of $0.94 \pm 0.64\ wt\%$ over the twenty-six pellets measured. Though the mean value is close to the percentage value ($1\ wt\%$) stated by the supplier, the large loading distribution is problematic when wanting to compare reaction rates between pellets. It was therefore decided to use the same pellet throughout the single pellet experiments.

Figure 5 compares the number frequency, percentage weight and available surface atoms of the nanoparticles of both 1% Pd/C pellets and 5% Pd/C powders used by Stamatiou and Muller (23). Assuming the nanoparticles are spherical, the number of surface atoms available for reaction per nanoparticle, N_s, is defined as;

$$N_s = \frac{A_{Pd}}{N_{atoms}} = 2\pi \left(\frac{d_{Pd}}{l_{unit}}\right)^2 \qquad (19)$$

Here N_{atoms} is the number of palladium atoms per nm^2, A_{Pd} is the surface area of the nanoparticle, d_p the diameter of the nanoparticle and l_{unit} the length of a palladium unit cell. The two size distributions are within the same magnitude but the 1% Pd/C pellet has a slightly larger average and boarder distribution (d_{50} pellets - 5.35 ± 1.99 nm) than the 5% Pd/C paste (d_{50} powder - 4.38 ± 1.27 nm).

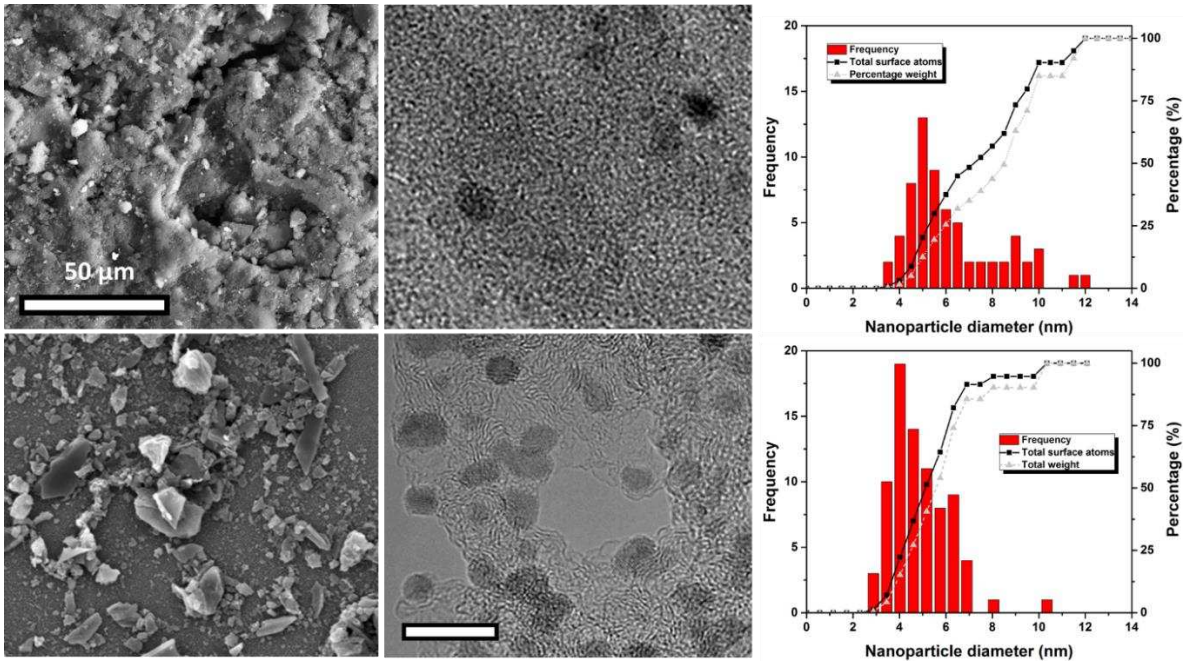

Figure 5: SEM image of the catalyst sample (left), TEM image of the palladium nanoparticles (middle) and the corresponding nanoparticle size distribution (right) of the 1% Pd/C pellets (top row) and 5% Pd/C (bottom row). The square and triangle trends represent the total surface atoms and weight of each bin respectively.

SEM images of the pellets and their respective elemental maps are shown in Figure 6. Both images show the palladium (coloured green) located in high concentration on the surface of the carbon support. The interior of the pellet on the other hand is overwhelmingly made up of carbon (coloured red). Pd linescan profiles for a cross section and surface of a 1% Pd/C pellet and the interior of a non-active carbon pellet is shown in Figure 7. Clearly the surface is strongly enriched in Pd. There is some variation over the surface scan, but the count is consistent at ~75. The linescan over the cross section of the pellet shows that the surface concentration is maintained to a depth of $\delta_s = 6\ \mu m$. Further in to the pellet the Pd concentration drops sharply by a factor 4 to 20 counts, and then more gradually as you progress further into the pellet interior. Interestingly, it never reaches the background scatter level that results from the scan of a pellet that is not impregnated with Pd.

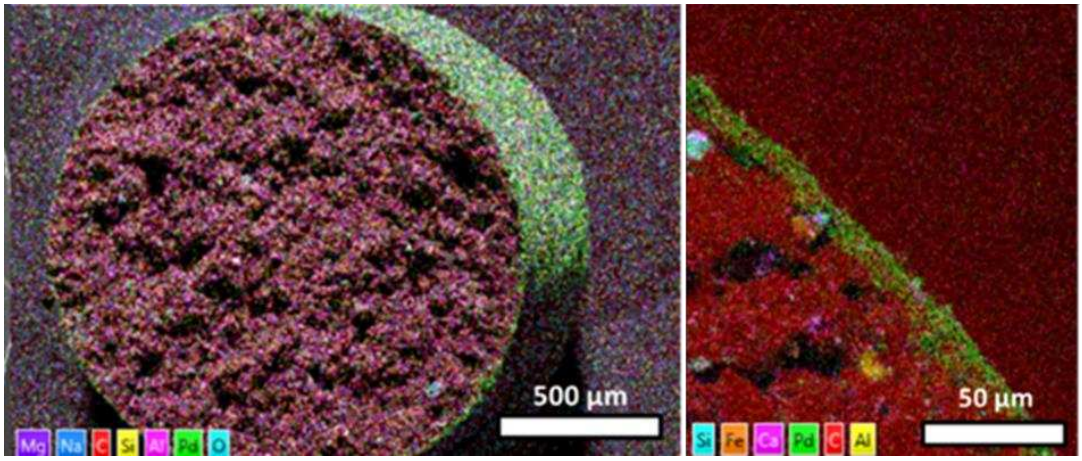

Figure 6: SEM images of a 1% Pd/C pellet and the corresponding EDX map showing the palladium (green) distribution over the exterior and interior of the pellet.

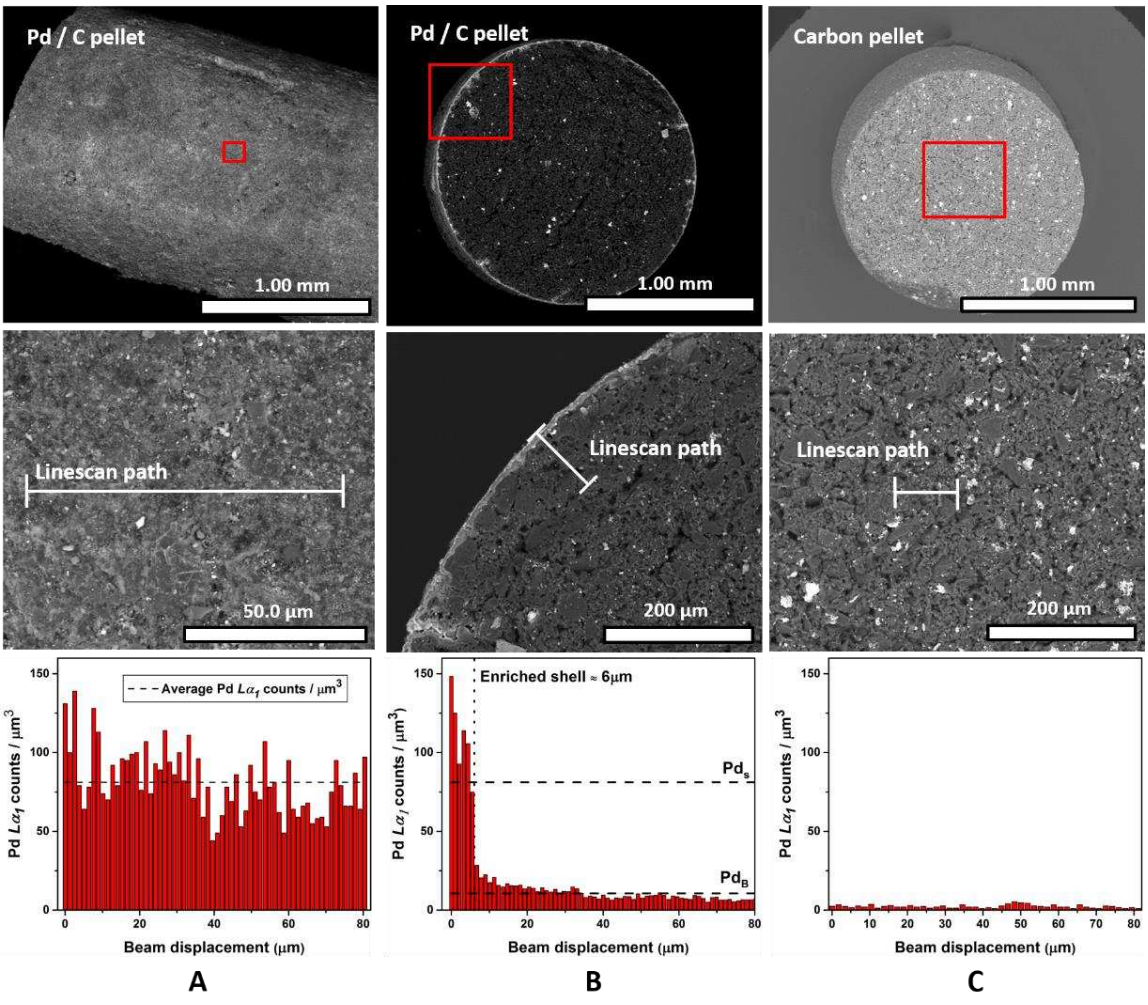

*Figure 7: SEM images of a 1 wt% Pd carbon pellet. (**A**) Surface of the pellet, (**B**) edge of a cross section and (**C**) centre of a cross section of the interior of an unloaded carbon pellet. **Top**: overview of*

the pellet with the location were a linescan was taken. ***Middle****: detailed view at the scale of the line scan and* ***Bottom****: the respective Pd count line scan profile. The palladium counts show a significant enrichment of the palladium count on the surface of the pellet.*

The linescan data allows estimation of the fraction of palladium $Pd_{\%S}$ in the shell with volume $2\pi r_p \delta_s L_p$, vs the fraction of palladium in the core of the pellet (volume $\pi r_p^2 L_p$). It was assumed that the count intensity remains constant across the diameter of the pellet once past the enriched shell region. Assuming a linear correlation between count $\#_{Pd}$ and concentration Pd:

$$Pd_{\%S} = \frac{\#_{Pd_s} \cdot 2\delta_s}{\#_{Pd_{shell}} \cdot 2\delta_s + \#_{Pd_{Core}} \cdot r_P} \qquad (20)$$

Using Eq. 20 the proportion of palladium in the shell was estimated to be 15.5% suggesting a large proportion of the palladium metal is located at low concentration within the interior of the pellet.

4.2 Bed porosity, liquid holdup and residence time

The bed porosity, ϵ_B of the reactor when fully packed was determined to be 39%. The residence time, τ (Figure 8) was calculated using Eq. 21 for liquid superficial velocities up to 0.0025 m s^{-1} (flow rates of 0.25 – 4.5 mL min^{-1}) (20). Here, φ is the volumetric flow rate, z_B the bed length and S the reactor cross-sectional area. Assessing the literature, Dudukovic *et al.* suggests that generally trickle bed reactors are operated with a liquid holdup of between 0.05-0.25 and liquid mass velocities of up to 50 kg m^2 s^{-1} (24). From the flow map generated by Sie and Krishna, to operate in the trickling flow regime liquid superficial mass velocities need to be < 10 kg m^2 s^{-1} for the superficial gas flow rate used (0.15 m s^{-1}) (25). Therefore, comparing this to the holdup data obtained, superficial liquid mass flow rates up to 0.25 kg m^2 s^{-1} (0.25 – 1 mL min^{-1}) were investigated.

$$\tau = \frac{\epsilon_B * \left[\beta_{Dyn} + \beta_{st}\right]}{\varphi} * z_B * S \qquad (21)$$

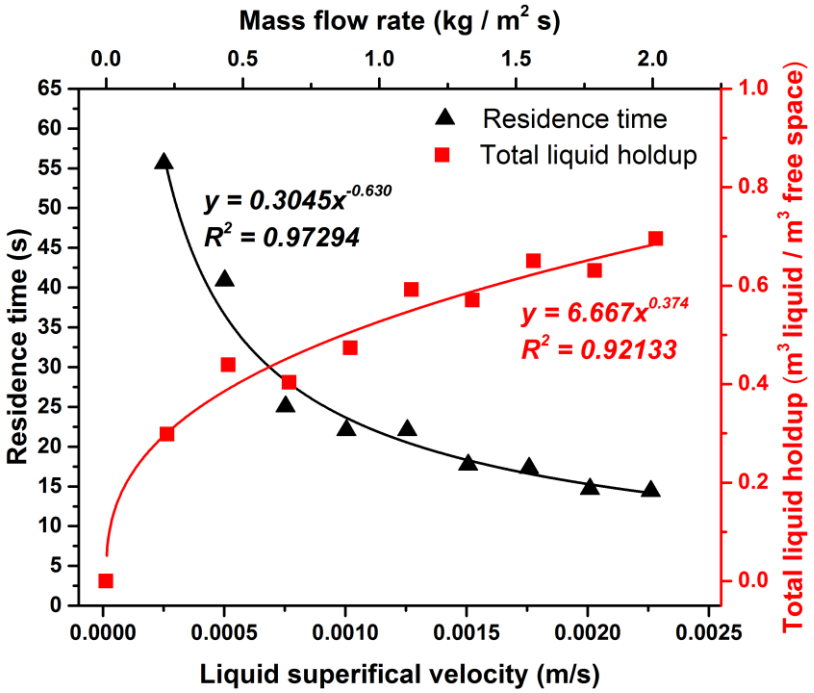

Figure 8: Liquid residence time and holdup in the single pellet reactor at flow rates between 0-10 mL min^{-1}, conducted at 21 °C, atmospheric pressure and 300 mLmin^{-1} gas flow rate.

4.3 Liquid film thickness

Figure 9 compares the experimentally measured film thicknesses to those predicted by the thin film and the general model. Both the thin film and general model fit the asymptotic nature of the experimental data obtained in this study well, with the thin film approach appearing to be more suitable at lower flow rates and the general model at higher flow rates. This is consistent with work for liquid flow on thin wires (26), where the disparity between thin films and films where $\delta \sim r_p$ was experimentally observed. For comparison, film thickness predicted for flow over spherical catalysts using the model proposed by Satterfield *et al.*(6) is also presented. Film thickness over pellets roughly a factor of two larger then films on spherical particles.

At the liquid flow rates investigated in the single pellet reactor the thin film and general model converge. For convenience the thin film model (Eq. 2) was therefore used to calculate the film thickness.

Using the calculated film thicknesses, the liquid residence time on a single pellet, $t_{residence\ pellet}$ was estimated using Eq. 22, assuming complete wetting of the pellet and is plotted in Figure 9.

$$t_{residence\ pellet} = \frac{A_p \delta}{\varphi} \qquad (22)$$

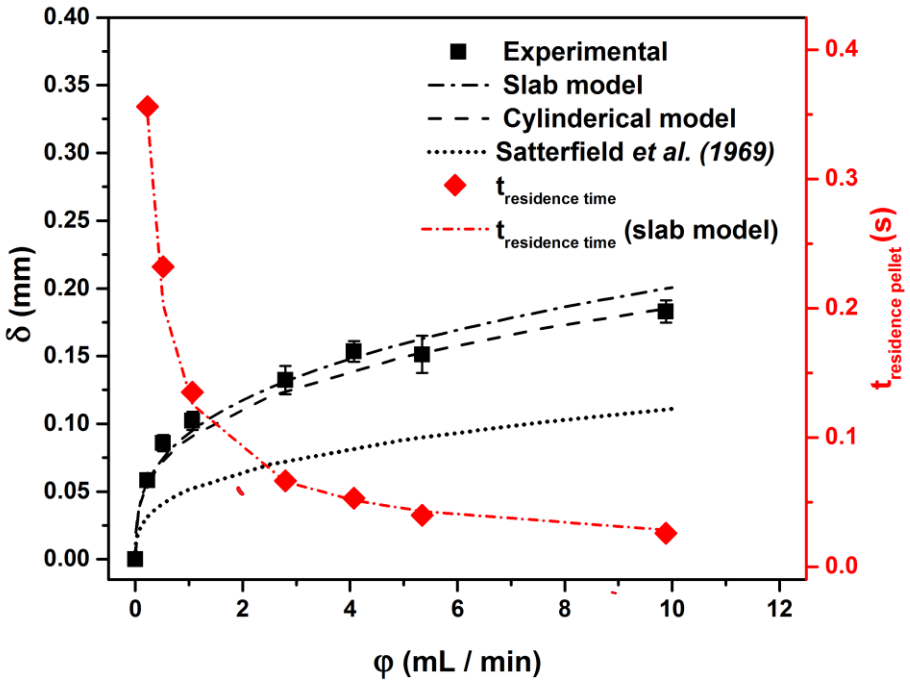

Figure 9: Comparison between the experimentally obtained film thicknesses and of those calculated from the slab and cylinder models for liquid flow rates between 0 – 10 mL min^{-1} at 1 bara and 21°C

4.4 Determination of the observed rate constant k''_{obs}

The intrinsic chemical reaction resistance Ω_R is a function of the observed rate constant, k''_{obs} and thus a value of the rate constant in the absence of pore resistance is required for proper determination of the overall mass transfer rate. It should be noted that k''_{obs} represents the observed reaction rate based on the external area of the pellet and is a function of temperature, styrene and hydrogen concentration. Therefore, we assume that these are essentially constant over the surface of the pellet.

To approximate k''_{obs} we use the observed rate constant reported by Stamatiou and Muller who used the same 5% Pd/C powder characterised and discussed in Section 4.1 for the hydrogenation of

styrene in an agitated slurry reactor (27). Based on the weight of palladium on the catalyst support and the hydrogen concentration in the fluid, C_f, an observed rate constant at 32 °C was determined;

$$\left(-R_{H_2}^{Pd}\right)/C_f = k_{obs}^{Pd} = 0.0273\frac{m^3(fluid)}{g(Pd).s} \qquad (23)$$

Comparing with the literature, the rate constant is larger than the rate of Nijhuis *et al*., who reported a rate constant of $0.0086\frac{m^3(fluid)}{g(Pd).s}$ for styrene hydrogenation on Pd/C (28). The lower rate constant is shown to be a result of active pore diffusion by the activation barrier reported by Nijhuis *et al*. The rate is of a similar order of magnitude to the rate reported by Meille *et al.* for α-methylstyrene hydrogenation using palladium on an alumina oxide support ($k_{obs}^{Pd} = 0.0106\frac{m^3(fluid)}{g(Pd).s}$) (29).

The SEM-EDX linescan of the pellet interior (Figure 7, Column B) shows that the pellets used in this study have an enriched palladium shell approximately 6 µm thick. The reaction rate of hydrogen in this enriched zone of the catalyst, $\left(-R_{H_2}^{Pd}\right)$ is defined as the moles of hydrogen consumed per second per gram of palladium present in the volume of enriched shell ($A_p\delta_{shell}$). Thus, the observed rate constant in the shell, k_{obs}^{Vshell} is defined as;

$$k_{obs}^{Vshell} = Pd_{\%S} \cdot W_p \cdot \frac{k_{obs}^{Pd}}{A_p\delta_{shell}} \qquad (24)$$

Using Eq. 24 the shell rate constant was found to be $2410\ \frac{m^3(fluid)}{m^3(shell).s}$. Here, $Pd_{\%S}$ is the fraction of palladium in the shell (Eq. 20), W_p the quantity of palladium in the pellet (grams), δ_{shell} is the thickness of the enriched shell and k_{obs}^{Pd} is the observed rate constant calculated from Eq. 24.Using the effective diffusion rate in Pd/C catalysts $D_{eff} = 2 \times 10^{-9}$m^2 s^{-1} determined by Kobayashi and Katsuzawa, the penetration depth of hydrogen in to the shell in the presence of the liquid phase can be approximated (30);

$$\frac{1}{M_T} = \frac{\sqrt{D_{eff}/k_{obs}^{V_{sh}}}}{\delta_{shell}} \qquad (25)$$

Using Eq. (25) the penetration depth was found to be ~16% of the enriched film thickness. Therefore, pore diffusion limits the reaction to a 1 µm thick surface layer on the pellet catalyst. Finally, the reaction rate per unit external pellet area, k_{obs}^{s}, results from k_{obs}^{Vsh} by multiplication with the volume ($A_p\delta_{shell}$) of the shell, and division by the total external interface (A_p):

$$k''_{obs} = \frac{1}{M_T} k_{obs}^{Vsh}\, \delta_{shell} = 0.0022\, \frac{m^3(fluid)}{m^2(external\ pellet\ surface).s} \qquad (26)$$

4.5 Two stage mass transfer model

The experimentally determined overall mass transfer rate of hydrogen, MTR''_{H2}, through the film is calculated from the increase in ethylbenzene concentration detected by offline gas chromatography:

$$MTR''_{H_2} = \frac{\varphi\ C_{ethylbenzene}}{A_p}\ in\ mol/s.m^2_{pellet} \qquad (27)$$

The effect of liquid flow rate on the overall mass transfer rate of hydrogen as a function of the liquid residence time over the surface of the pellet is illustrated in Figure 10. The absolute values of the experimental and modelled MTR''_{H_2} and the confidence intervals are given in Table 1. In both feed cases the rate was observed to vary significantly with liquid flow. The feed saturated with hydrogen gives significantly higher mass transfer rates compared to the hydrogen free feedstock. At the lower flow rates investigated, both datasets appear to begin moving towards the same asymptotic point. The decreasing trend observed in the hydrogen free feeds is thought to stem from the increase in film thickness (Eq. 2; $\delta \propto \sqrt[3]{\varphi}$). When the feed is saturated, the diffusional requirement is greatly reduced and thus the trend differs to that seen when the feed was hydrogen free.

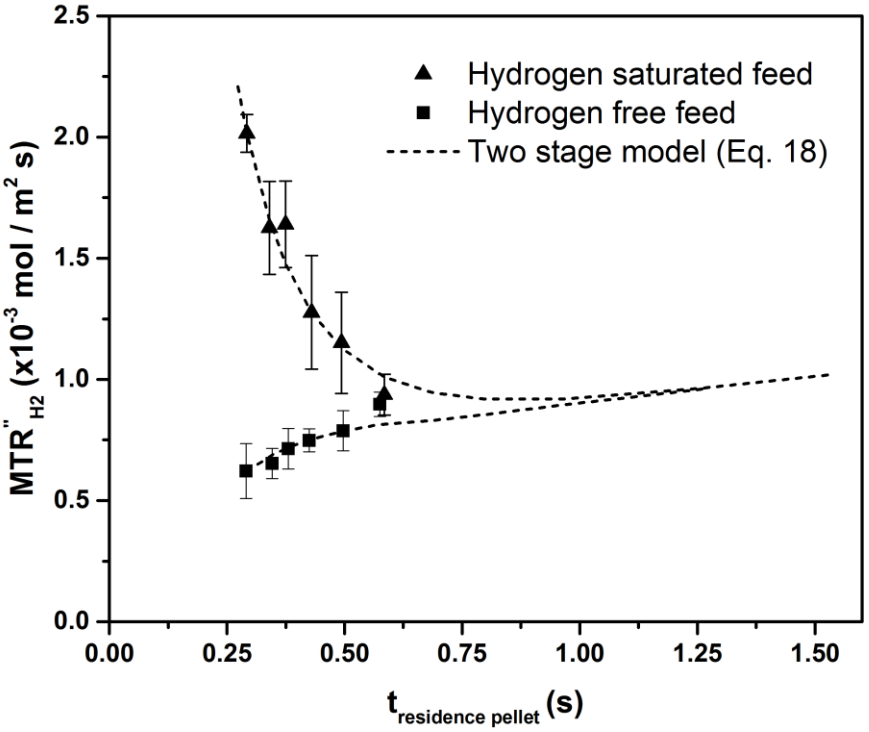

Figure 10: The effect of liquid flow rate as a function of liquid residence time on the pellet on the overall mass transfer rate of hydrogen with and without hydrogen saturated feed solutions. The experimental rates are compared with those predicted by the two stage mass transfer model.

Table 1: Upper and lower 95% confidence limits of the two stage mass transfer model for both hydrogen free and saturated feed cases.

	Pellet film residence time $t_{residence\ pellet}$ (s)	**Experimental MTR''_{H2} (x10^{-3} mol m^{-2} s^{-1})**	**Modelled MTR''_{H2} (x10^{-3} mol m^{-2} s^{-1})**	**Upper 95% confidence interval**	**Lower 95% confidence interval**
Hydrogen saturated feed	0.58	0.94	1.01	1.05	0.97
	0.49	1.15	1.13	1.17	1.09
	0.43	1.28	1.28	1.32	1.23
	0.37	1.64	1.48	1.52	1.43
	0.34	1.63	1.66	1.70	1.61
	0.29	2.02	2.02	2.06	1.97
Hydrogen free feed	0.57	0.90	0.81	0.86	0.77
	0.50	0.79	0.79	0.83	0.74
	0.42	0.75	0.75	0.79	0.71
	0.38	0.71	0.72	0.76	0.68
	0.35	0.65	0.69	0.73	0.65
	0.29	0.62	0.62	0.66	0.57

The results reported here differ from those of Satterfield *et al.* who studied the atmospheric hydrogenation of α-methylstyrene with a saturated hydrogen feed in reactor system consisting of 8 mm spherical pellets on a string (6). They observed dependence of the hydrogen consumption rate on flow rate only at and above 50 °C. We estimate their residence time on a pellet to range from 0.06 to 0.17 s, significantly shorter than for our case. Based on our model it is appears that the film over the spherical pellets was "flushed out" at low temperatures, and thus the system was reaction limited. As the reaction rate increases with temperature, the reaction resistance reduces, and the mass transfer resistances become noticeable. This results in the higher hydrogenation rates observed by Satterfield *et al.* at lower liquid velocities and hence thinner liquid films.

The five model parameters $\alpha, \gamma_1, \gamma_2, \gamma_3 and\ k_{b.ref}$, were fitted to the experimental mass transfer rates of hydrogen by minimising the Sum of Squares $\sum_{i=0}^{n}\left(y_{exp.i} - y_{calc.i}\right)^2$. The absolute values of the fitted and calculated parameters used in the two stage model are presented in Table 2. The model fits both the hydrogen saturated and free feed cases very well, falling within the upper and lower experimental error limits for all but one point. This suggests that the relative rate of hydrogen supply by both the liquid (convective) and mass transfer across the pellet surface (radial) are important factors. The predicted MTR''_{H_2} from the model also highlights the asymptotic behaviour the experimental data appears to be moving towards

Table 2: Values of the fitting and model parameters used in the two stage mass transfer model.

	Parameter	Value	Source / Comment
Bead section	$k_{b.ref}$	4.69x10^{-6} m s^{-1}	Mass transfer coefficient over the beads defined in Eq. 7.
	γ_1	-0.156	Gradient of the effect of flowrate on mass transfer to beads, defined in Eq. 7.
Pellet section	γ_2	1.86	Ratio of liquid film thickness over a pellet in a bed vs film thickness (δ) over a pellet stack.
	γ_3	65.5 %	Fraction of liquid flowing over the pellet (bypass factor)
	α	0.97	Fraction of the liquid film that forms the mass transfer resistance, defined in Eq. 11
Mass transfer resistances	$1/\Omega_f$	119 – 169x10^{-6} m s^{-1}	Gas to film transport resistance $\Omega_f = \delta\gamma_2/\mathbb{D}_{H_2}$
	$1/\Omega_{f-s}$	1350 – 1520x10^{-6} m s^{-1}	Film to catalyst surface transport resistance calculated from Eq. 12
	$1/\Omega_R$	2200x10^{-6} m s^{-1}	Chemical reaction resistance calculated from Eq. 26

Visual observation revealed that liquid was bypassing the pellet and based on the mass transfer data the liquid bypass factor, γ_3, was estimated to be 65%. Whereas this number could not be validated, it is consistent with the observations. The two stage model indicates that the falling film model is not truly representative of the film thickness around the pellet in the bed, as the thickness proportionality constant, γ_2, suggests the film is almost twice as thick as that predicted by the slab model. It does show, however, that the falling film model gives a reasonable estimate for the relationship between film thickness and flow. It does not account for the additional liquid holdup present on the pellet due to the proximity of the beads, nor are differences in the pellet position considered.

Mass transfer in the bead section: The estimated mass transfer coefficient for the beads section is in the right order of magnitude and is in good agreement when compared to systems involving gas absorption with no subsequent chemical reaction. This is evident when comparing the

experimentally derived Nusselt number with the well-established correlation involving the Reynolds and Schmidt numbers for a flat plate, both defined in Eq. 28 (31);

$$Nu_{bs} = \frac{k_{b.ref} N_{bs} d_{bs}}{\mathbb{D}_{H_2}} = 0.664\, Re_{bs}^{1/2} Sc^{1/3} \text{ with } Re_{bs} = \frac{\rho U_{bs} N_{bs} d_{bs}}{\mu} \text{ and } U_{bs} = \frac{\varphi}{2\pi d_{bs}\, \delta_b} \quad (28)$$

Where δ_b is the liquid film thickness over the surface of the beads (considered here as a cylinder as illustrated in Figure 3) and is calculated using the cylindrical film thickness model (Eq. 4). The experimentally derived and correlated Nusselt numbers were determined to be 40 and 52 respectively, with the difference due to the fact the geometries are different.

The mass transfer rate, $k_{b.ref}$, is used to determine the hydrogen concentration at the point where the liquid contacts the pellet, C_0, as a function of flow rate (Eq. 10, Figure 11). At lower flowrates, more time is available for mass transfer, and the concertation, C_o, at the pellet approaches equilibrium at the reaction conditions (1 bara). At higher flow rates and short liquid residence times, the system is essentially flushed out and C_o approaches the feed concentration.

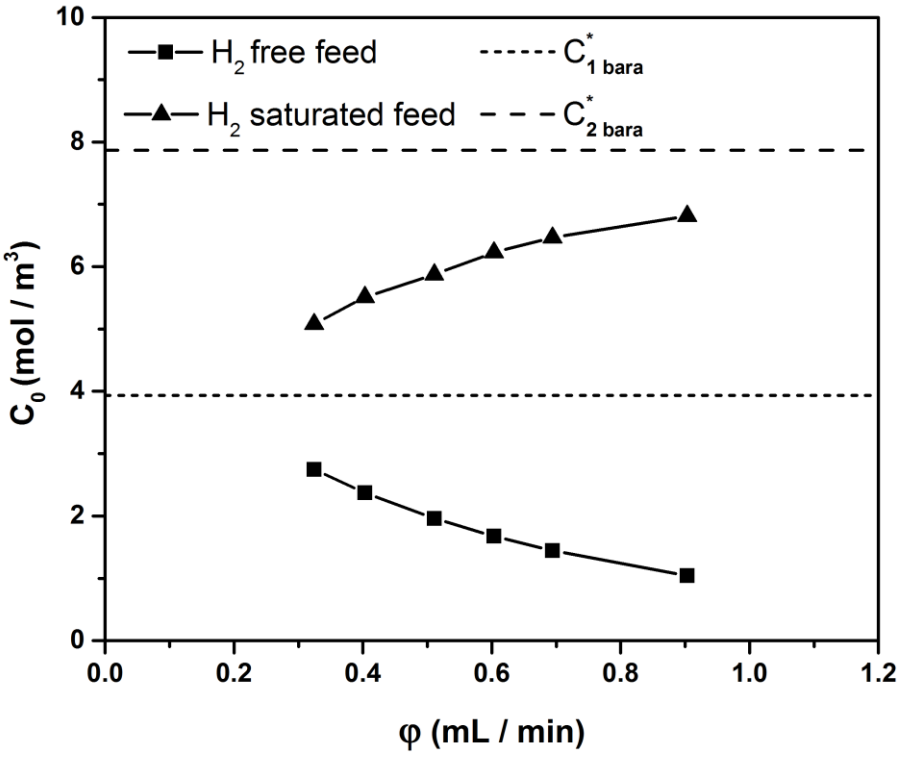

Figure 11: The calculated hydrogen concentration in the liquid when it reaches the pellet, C_0 for both the hydrogen saturated and hydrogen free feed experiments. The dashed and dotted lines represent the saturated feed concentration and the equilibrium concentration of hydrogen in the liquid respectively.

Mass transfer to the pellet: The gas to film mass transfer coefficient ($1/\Omega_f$) was found to be an order of magnitude larger than that of the beads. Moreover, gas film mass transport resistance barrier consists of 97% of the film. The calculated mass transfer coefficient is in the same order of magnitude but slightly lower than gas-liquid coefficients reported in the literature (32, 33) for trickle bed reactors investigated at similar superficial liquid flow rates (between $3 - 4\ x\ 10^{-5}$ m s^{-1}). The resistance for hydrogen transport from the film to the surface of the catalyst is thus small as the distance to diffuse is small. The corresponding mass transfer coefficient ($1/\Omega_{f-s}$) and the reaction rate constant, k''_{obs} ($= 1/\Omega_R$), are both an order of magnitude larger than the mass transfer rate from the gas phase. This would suggest that mixtures of active and inactive catalyst can convert more raw material per unit mass of palladium as a result of additional non active mass transfer area.

The concentration gradient over the pellet is shown in Figure 12 for hydrogen free and saturated feed solutions at the maximum and minimum feed flowrates. As the flow progresses along the length of the pellet, L_p, the hydrogen concentration moves to an asymptotic value. If we consider the case of having a very large pellet $(L_p \to \infty)$ the film concentration reaches C_∞ (Eq 15). The film reaches equilibrium relatively quickly, but the extent to which the liquid is saturated C_0 still has a large impact on the overall mass transfer rate as film to catalyst resistance is very small.

When the flowrate increases the film will reach the hydrogen concentration of the feed, and the term A_0/A_P tends to zero. As a result, the hydrogen concentration of the film approaches C_o. This will result in the highest hydrogen conversion rates per unit mass of palladium, but the concentration of product downstream will reduce.

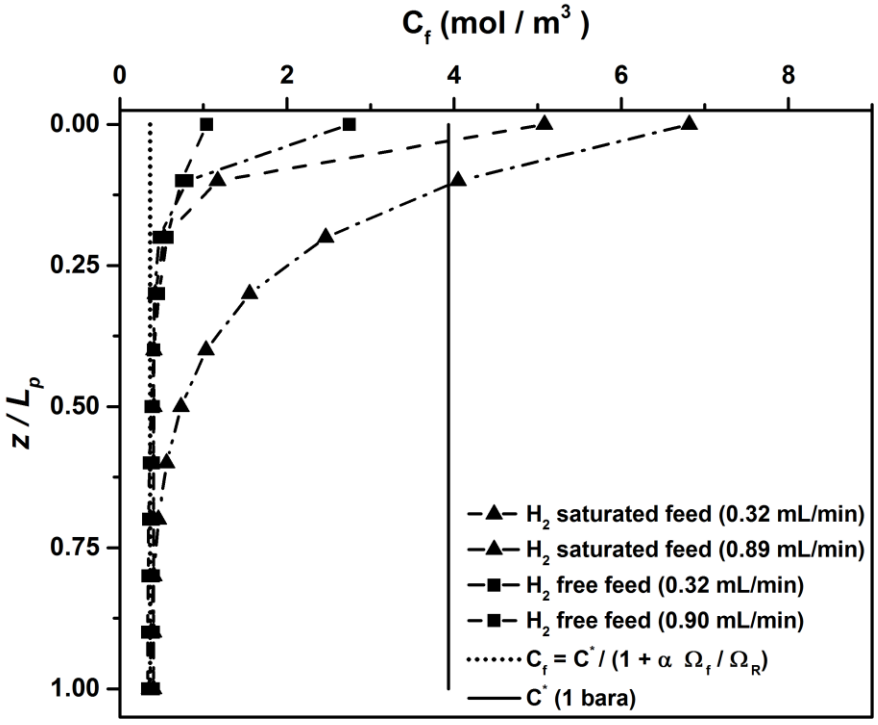

Figure 12: Diagram illustrating the change in concentration of hydrogen in the liquid film over the area of a pellet calculated using Eq 15 for both hydrogen free and saturated feed solutions at the maximum and minimum feed flowrates. The dotted line highlights the case where $A_p \rightarrow \infty$.

One of the key objectives of this paper is to establish the relative contributions of hydrogen transport from (i) convective transport of hydrogen with the liquid flowing onto the pellet MTR''_{conv}, and (ii) radial mass transfer of hydrogen from the gas phase to the liquid film surrounding the pellet, MTR''_{radial}.

The convective transport may be estimated from the concentration difference between the liquid entering the pellet and the liquid leaving the pellet. The radial mass transfer is then the difference between the total mass transfer observed, and the contribution of convection:

$$MTR''_{radial} = MTR''_{H_2} - MTR''_{conv} \quad with \quad MTR''_{conv} = \varphi\gamma_3(C_0 - C_f) \tag{29}$$

Figure 13 compares the two modes of hydrogen delivery to the pellet for all flowrates and feed conditions. The overall mass transfer rate is significantly affected by convective transport, evident by the fact that as the molar flow of hydrogen increases the rate at which hydrogen is consumed

increases. As illustrated in Figure 12, the film concentration C_f will always eventually reach C_∞, irrespective of the feed conditions or flow rates used. Therefore, the differentiator between two feed conditions is the convective contribution, and it is only at very low flow rates that the convective and radial contributions for the two feed conditions become comparable.

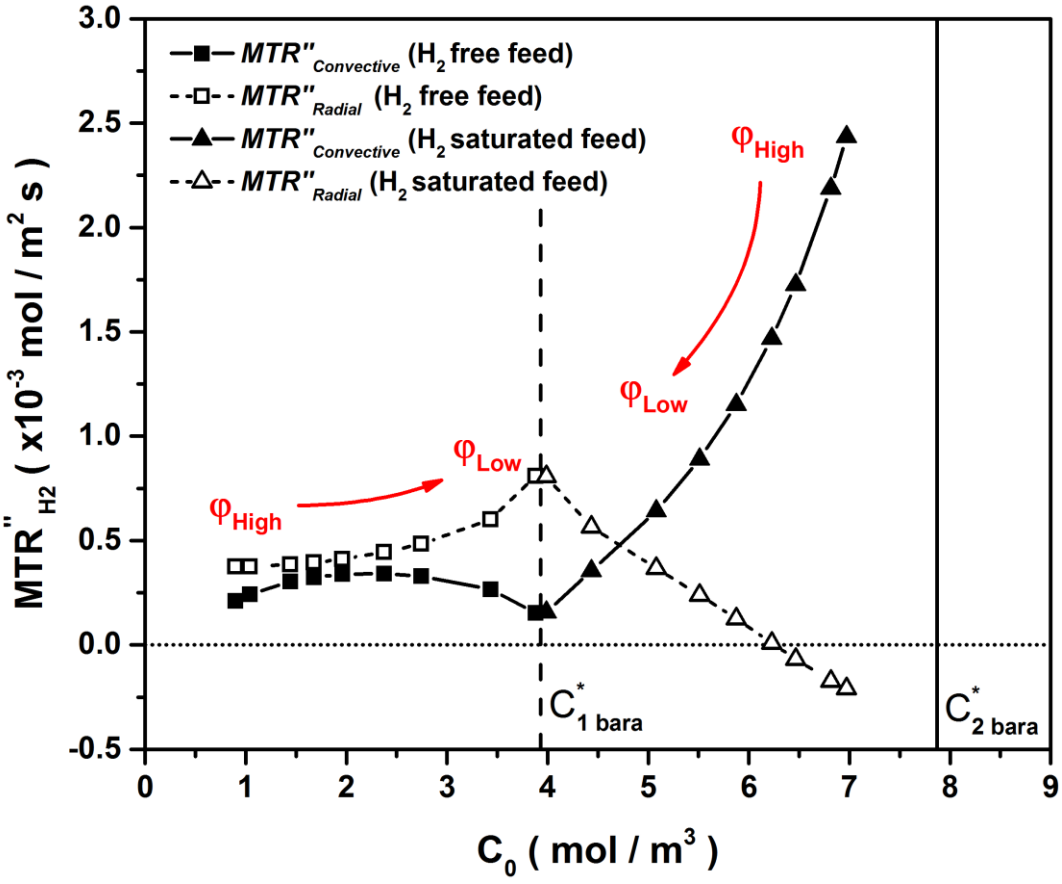

Figure 13: Comparison between the convective transport of hydrogen into the pellet from the glass beads and the radial transfer of hydrogen from the gas to the liquid for both feed conditions and all flow rates investigated. φ_{High} and φ_{Low} refer to the velocity of the liquid phase for each feed condition.

5 Conclusions

The ability to manipulate the average concentration of hydrogen close to the surface of the pellet is a valuable tool in the manufacture of fine chemicals. Specifically, being able to control the quantity of hydrogen accessible to a substrate which often results in the improved selectivity of a reaction. A

scaled down trickle bed reactor consisting of single 1% Pd/C pellet immobilized in glass beads was used to investigate the overall mass transfer rate of hydrogen during the hydrogenation of styrene.

Experimental observations show a large difference in the transfer rate of hydrogen to the pellet when operating with feeds free of hydrogen, and feeds saturated with hydrogen. Mass transfer also changed dramatically with flowrate. A two stage mass transfer model was proposed and fit to the experimental data to describe and compare the two mechanisms by which hydrogen is supplied to the pellet: (i) convective transport of hydrogen with the liquid flowing onto the pellet and (ii) radial mass transfer of hydrogen from the gas phase to the liquid film surrounding the pellet.

The model can reconcile the data from both saturated and hydrogen free feeds and demonstrates that delivery of hydrogen via radial mass transfer is relatively constant when the convective flux of hydrogen is low. When the convective flux of hydrogen increases (by super saturation of the feed and higher flowrates) the rate of hydrogen consumption increases virtually proportional to the hydrogen flux, indicating that most of the hydrogen transported by convection is consumed. As the hydrogen concentration in the film on the pellet increases, the radial mass transfer reduces, and even becomes negative when operating a saturated feed at high flowrates.

The results from this work demonstrate that by controlling the ratio of inactive to catalytically active surface area in a trickle bed reactor, one can control the hydrogen concentration close to the surface of the catalyst pellets. This methodology could be readily extended to many other three phase catalytic processes whereby transport of the gaseous reacting molecules limits the overall rate of reaction. Involving not only the hydrogenation of fine chemicals but hydrogenolysis reactions during hydrodesulfurization, catalytic oxygenation of alcohols such as ethanol and even find application in specific bioreactions such as gas synthesis of methanol from hydrogen and carbon monoxide.

The knowledge of how to better regulate the supply of hydrogen gas to the catalyst and manipulate the mass transfer characteristics, unlocks the potential of trickle bed reactors, making them an attractive technology for the manufacture of fine chemicals in the agrochemical and pharmaceutical

industries. Solving this problem paves the way to further understanding and cracking the complex scale up and selectivity issues involved in three phase reactions whilst capitalising on the benefits continuous processing offers.

Acknowledgments

The generous support by Syngenta, the EPSRC Centre of Doctoral training in Complex Particulate Products and Processes (Grant number EP/L015285/1) is acknowledged.

References

1. S. McGovern, G. Harish, C.S., Pai, W. Mansfield, J.A. Taylor, S. Pau and R.S. Besser, Multiphase flow regimes for hydrogenation in a catalyst-trap microreactor, Chem. Eng. J. 135 (2008) S229-S236. https://doi.org/10.1016/j.cej.2007.07.055
2. J.G.V. Alsten, M.L. Jorgensen and D.J. am Ende, Hydrogenation of a Pharmaceutical Intermediate by a Continuous Stirred Tank Reactor System, Org. Process Res. Dev. 13 (2009) 629-633. https://doi.org/10.1021/op800170r
3. F.S. Medoras, J. Ancheyta and J. Chen, Review on criteria to ensure ideal behaviors in trickle-bed reactors, Appl. Catal. A-Gen. 355 (2009) 1-19. https://doi.org/10.1016/j.apcata.2008.11.018
4. E.H. Stitt, Alternative multiphase reactors for fine chemicals: A world beyond stirred tanks, Chem. Eng. J. 90 (2002) 47-60. https://doi.org/10.1016/S1385-8947(02)00067-0
5. H. Gierman, Design of laboratory hydrotreating reactors: Scaling Down of Trickle-flow Reactors, Appl. Catal. 43 (1988) 277-286. https://doi.org/10.1016/S0166-9834(00)82732-3
6. C.N. Satterfield, A.A. Pelossof and T.K. Sherwood, Mass transfer limitations in a trickle-bed reactor, AlChE J. 15 (1969) 226-234. https://doi.org/10.1002/aic.690150219
7. T. Bauer and S. Haase, Comparison of structured trickle-bed and monolithic reactors in Pd-catalyzed hydrogenation of alpha-methylstyrene, Chem. Eng. J. 169 (2011) 263-269. https://doi.org/10.1016/j.cej.2011.02.033

8. S. Haase, M. Weiss, R. Langsch, T. Bauer and R. Lange, Hydrodynamics and mass transfer in three-phase composite minichannel flow reactors, Chem. Eng. Sci., 94 (2013) 224-23. https://doi.org/10.1016/j.ces.2013.01.050
9. R. Langsch, S. Haase and R. Lange, Hydrodynamics and mass transfer in a pellet string reactor for gas–liquid–solid reactions, Chem. -Ing. -Tech., 85 (2013) 642-655. DOI:10.1002/cite.201200189
10. R. Langsch, J. Zalucky, S. Haase and R. Lange, Investigation of a packed bed in a mini channel with a low channel-to-particle diameter ratio: Flow regimes and mass transfer in gas–liquid operation, Chem, Eng. Process, 75 (2014) 8-18. https://doi.org/10.1016/j.cep.2013.10.004
11. L.E. Kallinikos and N.G. Papayannakos, Intensification of hydrodesulphurization process with a structured bed spiral mini-reactor, Chem. Eng. Process 49 (2010) 1025-1030. https://doi.org/10.1016/j.cep.2010.07.007
12. A. Hipolito, M. Rolland, C. Boyer and C. De Bellefon, Single pellet string reactor for intensification of catalyst testing in gas/liquid/solid configuration, Oil Gas Sci. Technol. 65 (2010) 687-701. DOI: 10.2516/ogst/2009079
13. J.R. Balder and E.E. Petersen, Application of the single pellet reactor for direct mass transfer studies: I. Mass transfer in porous media, J. Catal. 11 (1968) 195-201. https://doi.org/10.1016/0021-9517(68)90032-8
14. 10. J.R. Balder and E.E. Petersen, Application of the single pellet reactor for direct mass transfer studies: II. Measurement of composition at center of catalyst pellet, J. Catal. 11 (1968) 202-210. https://doi.org/10.1016/0021-9517(68)90033-X
15. L.L. Hegedus and E.E. Petersen, An Improved Single-Pellet Reactor to Study the Interaction of Kinetics with Mass Transfer Effects in Heterogeneous Catalysis, Ind. Eng. Chem. Fundamen. 11 (1972) 579-584. https://doi.org/10.1021/i160044a025
16. J. Adaje and M. Sheintuch, Comparison of multiplicity patterns of a single catalytic pellet and a fixed catalytic bed for ethylene oxidation, Chem. Eng. Sci. 45 (1990) 1331-1342. https://doi.org/10.1016/0009-2509(90)87125-C

17. P.C. Watson and M.P. Harold, Dynamic effects of vaporization with exothermic reaction in a porous catalytic pellet, AlChE J. 39 (1993) 989-1006. https://doi.org/10.1002/aic.690390609
18. M. Aygün, T.W. Chamberlain, M.D.C. Gimenez-Lopez and A.N. Khlobystov, Magnetically recyclable catalytic carbon nanoreactors, Adv. Funct. Mater. 28 (2018), 1802869. https://doi.org/10.1002/adfm.201802869
19. S. Lin and W. Liu, Instability of film coating of wires and tubes, AlChE J. 21 (1975) 775-782. https://doi.org/10.1002/aic.690210420
20. D. Stegeman, F.E.V. Rooijen, A.A. Kamperman, S. Weijer and K.R. Westerterp, Residence time distribution in the liquid phase in a cocurrent gas-liquid trickle bed reactor, Ind. Eng. Chem. Res, 35 (1996), 378-385. https://doi.org/10.1021/ie940455v
21. Q. Liu, F. Takemura and A. Yabe, Solubility of hydrogen in liquid methanol and methyl formate at 20 C to 140 C, J. Chem. Eng. Data 41 (1996) 1141-1143. https://doi.org/10.1021/je9601321
22. O. Levenspiel, Chemical Reaction Engineering, Third Ed., John Wiley & Sons, New York, 1999.
23. I.K. Stamatiou and F.L. Muller, Determination of mass transfer resistances of fast reactions in three-phase mechanically agitated slurry reactors, AlChE J. 63 (2017) 273-282. https://doi.org/10.1002/aic.15540
24. M.P. Dudukovic, Ž.V. Kuzeljevic, D.P. Combest, Three-Phase Trickle-Bed Reactors, Ullmann's Encyclopedia of Industrial Chemistry, Wiley-VCH Verlag GmbH & Co.KGaA, Weinheim, 2014, pp. 1–40. https://doi.org/10.1002/14356007.b04_309.pub2
25. S. Sie and R. Krishna, Process development and scale up: III. Scale-up and scale-down of trickle bed processes, Rev. Chem. Eng. 14 (1998) 203-252. https://doi.org/10.1515/REVCE.1998.14.3.203
26. J. Grünig, T. Skale and M. Kraume, Liquid flow on a vertical wire in a countercurrent gas flow, Chem. Eng. J. 164 (2010) 121-131. https://doi.org/10.1016/j.cej.2010.08.040

27. I. Stamatiou, C. Brennan and F.L. Muller, Determination of styrene hydrogenation surface kinetics through detailed simulation of the hydrogen uptake curve, React. Chem. Eng. (2019) 4 1477-1485.
28. T.A. Nijhuis, F.M. Dautzenberg and J.A. Moulijn, Modeling of monolithic and trickle-bed reactors for the hydrogenation of styrene, Chem. Eng. Sci. 58 (2008) 1113-1124. https://doi.org/10.1016/S0009-2509(02)00547-X
29. V. Meille, C. de Bellefon and D. Schweich, Kinetics of α-Methylstyrene Hydrogenation on Pd/Al2O3, Ind. Eng. Chem. Res. 41 (2002) 1711-1715. https://doi.org/10.1021/ie010460g
30. J.I. Kobayashi and H. Katsuzawa, The geometrical evaluation of effective diffusion coefficient in the liquid phase for porous bodies consisting of spherical elementary particles, Can. J. Chem. Eng. 64 (1986) 419-425. https://doi.org/10.1002/cjce.5450640309
31. T.K. Sherwood, R.L. Pigford and C.R. Wilke, Mass Transfer, Second Ed., McGraw-Hill Inc., USA, 1975, Chapter 3; Rate equations for molecular diffusion.
32. K. Metaxas and N. Papayannokos, Gas-Liquid Mass Transfer in a Bench-Scale Trickle Bed Reactor used for Benzene Hydrogenation, Chem. Eng. Technol. 31 (2008) 1410-1417. https://doi.org/10.1002/ceat.200800107
33. I. Stamatiou and F.L. Muller, Determination of mass transfer resistances in trickle bed reactors, Chem. Eng. J. 377 (2019) 119808. https://doi.org/10.1016/j.cej.2018.08.194